

Microstructure and properties of an infra-red transmitting chalcogenide glass-ceramic

J. J. MECHOLSKY JUN*, C. T. MOYNIHAN, P. B. MACEDO,
G. R. SRINIVASANT†

Chemical Engineering and Materials Science Department, Catholic University of America, Washington, D.C., USA

A chalcogenide glass-ceramic ($0.3 \text{ PbSe}-0.7 \text{ Ge}_{1.5} \text{ As}_{0.5} \text{ Se}_3$) which transmits in the infra-red region between 8 and $12 \mu\text{m}$ was produced from a phase separated parent glass. The glass transition temperature (T_g) was increased from 280 to $\sim 340^\circ\text{C}$ by crystallizing the phase with the lower T_g . Further heat-treatment produced a glass-ceramic that was up to 60% crystalline and contained PbSe, PbSe₂ and GeSe₂ crystals with a gran size of $\sim 0.5 \mu\text{m}$. The infra-red transmission of the glass-ceramic decreased with increased crystallinity. The glass-ceramic modulus of rupture (38 MN m^{-2}) was increased to as much as twice that of the glass and the Vickers hardness increased by 30% to $\sim 280 \text{ kg mm}^{-2}$.

1. Introduction

There has been increasing interest in strong materials transparent in the infra-red up to $12 \mu\text{m}$. A number of materials have been considered as candidates for infra-red laser windows [1]; alkali halides, KCl in particular [2-4], hot-pressed or vapour-deposited polycrystalline materials such as ZnSe [3, 4] and chalcogenide glasses [5]. The possibility that fine grained polycrystalline chalcogenides produced by a glass-ceramic process would meet both the absorption and strength requirements of such a window led to this study. This paper describes the development and properties of a prototype infra-red transparent chalcogenide glass ceramic in the Pb-As-Ge-Se system.

The chalcogenide glass-ceramic requires small crystalline regions ($< 10 \mu\text{m}$) to avoid light scattering [8] and small finely dispersed crystals for high strength [9]. The authors suggest that this can be accomplished by selecting a glass that transmits infra-red radiation and which can be phase separated by additions of metallic chal-

cogenides. The homogeneous glass $\text{Ge}_{3.3} \text{ As}_{1.2} \text{ Se}_{5.5}$ has excellent infra-red properties [10] and one of the highest glass transition temperatures (353°C) [11] of the chalcogenides. Our early studies [6, 7] indicated that a PbSe addition to this approximate composition produced small, interconnected microstructure. Further experiments were conducted on this system to determine the immiscibility-liquidus diagram [12]. On the basis of these previous studies the composition 30 mol % PbSe-70 mol % $\text{Ge}_{1.5} \text{ As}_{0.5} \text{ Se}_3$ was selected for this investigation. This paper describes the effect of microstructural changes and crystallization on the optical and mechanical properties of this glass.

2. Experimental procedures

2.1. Heat-treatment

$0.3 \text{ PbSe}-0.7 \text{ Ge}_{1.5} \text{ As}_{0.5} \text{ Se}_3$ specimens were prepared by melting stoichiometric amounts of the constituent elements in approximately 20 g batches, as described previously [12], quenching in air, and subsequently heat-treating the samples

*Present address: Naval Research Laboratory, Washington, D.C.20375, USA.

†Present address: International Business Machines Corporation, Hopewell Junction, N.Y. 12533, USA.

for extended periods of time above the glass transition temperature, T_g .

The heat-treatments above the glass transition temperature to promote and control crystallization during glass-ceramic formation from the glass were performed both in one and two stages.

2.2. Electron microscopy

Electron microscopy studies were carried out on single-stage and two-stage carbon replicas in an A.E.I. (EM802) microscope. In several cases, small chips of samples adhered to the carbon replica. This made possible direct transmission electron microscopy and electron diffraction studies of these samples. Samples were also thinned by ion etching* using argon ions at 6 kV on two opposite surfaces of a 4 mil thick sample. These samples were observed in direct transmission and in dark field illumination. The crystal diffraction patterns were observed using selected-area diffraction. Volume fraction measurements were made using enlarged photographs of several electron micrographs by cutting out and weighing the areas of the photographs corresponding to the respective phases. The errors involved in this method arise chiefly from difficulties in differentiation of the two phases on the micrograph. Particle size determinations were also made on these micrographs by the linear intercept method [13].

2.3. X-ray diffraction

Powder X-ray diffraction patterns (Debye-Scherrer camera) were taken of amorphous and crystalline specimens which had been freshly powdered with a mortar and pestle.

2.4. DSC

The glass transition temperatures of amorphous and partially amorphous samples were measured using a differential scanning calorimeter (DSC)† A heating rate of $+20 \text{ K min}^{-1}$ was used. The glass transition temperature, T_g , was defined as the extrapolated onset of the rise in the heat capacity. The occurrence of two endothermic rises in the heat capacity of a phase-separated material was taken to indicate two glass transition temperatures, one for each glassy phase present [6, 7].

2.5. Infra-red transmission

Specimens of 1 cm o.d. were cut into various thicknesses ranging from 0.05 to 1 cm. These samples were sealed into Vycor tubes and given heat-treatments similar to those of the samples used for phase and immiscibility studies. The opposite faces of the samples were then polished plane parallel and the infra-red spectra recorded.‡

2.6. Microhardness measurements

Vickers' microhardness measurements (50 and 100 g loads) were made on the samples used for infra-red transmission. Five or six indentations were made per specimen.

2.7. Mechanical strength

Sample bars of $0.3 \text{ PbSe}-0.7 \text{ Ge}_{1.5} \text{ As}_{0.5} \text{ Se}_3$, both annealed and heat-treated, were tested in air at 40% r.h. on a three-point bend test fixture on a tensile testing machine§ with a head drive speed of 7.6 cm sec^{-1} . The samples were typically 0.25×0.5 cross-section with span lengths of approximately 1 cm. The surfaces had been ground parallel to the longitudinal axis with a diamond wheel of 180 grit at a grinding speed of approximately 1 cm sec^{-1} .

All fracture surfaces were examined and fracture mirror measurements were made when possible. The outer mirror, i.e. the demarcation between the mist and hackle, was used in calculations of fracture energy [14, 15].

3. Results and discussion

3.1. The effect of heat-treatment on microstructure and composition

The $0.3 \text{ PbSe}-0.7 \text{ Ge}_{1.5} \text{ As}_{0.5} \text{ Se}_3$ composition was selected for further study of effects of heat-treatment and crystallization because it forms a glass of small interconnected microstructure upon air quenching. The selection of the composition near the centre of the immiscibility dome [12] insured nearly equal volume fractions of the two phases, and the presence of large amounts of $\text{Ge}_{1.5} \text{ As}_{0.5} \text{ Se}_3$ prevents immediate crystallization upon quenching [16].

Fig. 1 shows an electron micrograph of the glass, air quenched from a melting temperature of

*Ion Micro Milling Instrument, Commonwealth Scientific, Inc. Alexandria, Virginia, USA.

†Perkin-Elmer Model DSC-1B.

‡Perkin-Elmer Model 467 Spectrophotometer.

§Ametek.

DSC Trace of $0.3\text{PbSe} - 0.7\text{Ge}_{1.5}\text{As}_{0.5}\text{Se}_3$
Glass Quenched from Melt

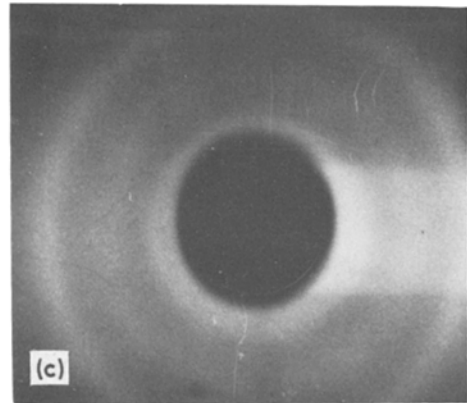
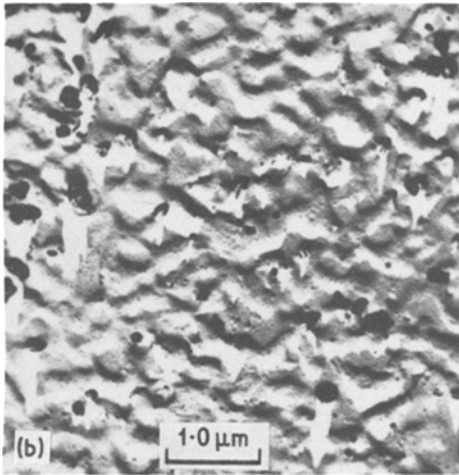
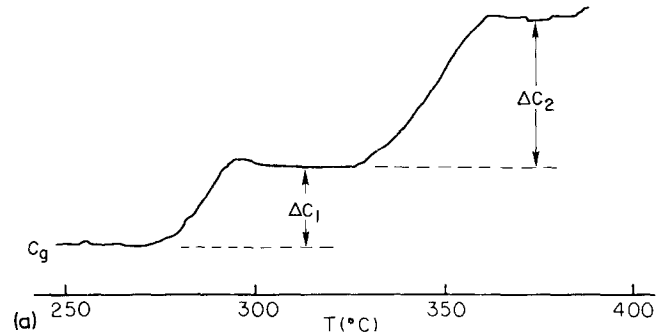


Figure 1 $0.3\text{PbSe}-0.7\text{Ge}_{1.5}\text{As}_{0.5}\text{Se}_3$ glass air quenched from melt. Change of slope in the DSC trace indicates two glass transition temperatures, at 280 and 325° C. (b) Two stage replication. (c) X-ray diffraction.

850° C. The initial microstructure in this glass is interconnected (a 0.33 to 0.67 volume fraction ratio of the amorphous phases) and shows secondary phase separation in at least one phase. This initial microstructure is probably due to a structure that is formed during quenching from the melt. A DSC trace shows two heat capacity breaks indicating two glass transition temperatures, at about 280 and 325° C, corresponding to the two phases seen in the micrograph in Fig. 1. DSC studies as a function of composition [7] have shown that the low T_g (280° C) is associated with the PbSe-rich phase, while the high T_g is associated with the PbSe-poor phase. The X-ray diffraction pattern of Fig. 1 with two diffuse rings is typical for glassy materials (the closest ring to the centre is from incomplete blocking of the transmitted beam).

Fig. 2 shows that at very early stages of heat-treatment (3 h at 350° C), only one phase in-

itially is crystalline; these crystals are small (500 Å) and consist of lead selenide in two stoichiometric forms (PbSe and PbSe₂) as determined from X-ray data. One phase has regular spherical secondary glassy particles and the other phase has irregularly shaped crystals. Fig. 2 also shows a dark-field micrograph which reveals the small irregularly shaped crystals in only one phase.

Fig. 3 shows micrographs and a DSC trace after heat-treatment at 350° C for 65 h or longer. The size of the microstructure (~0.7 μm) has still not changed greatly from that of Fig. 1, although it has lost its interconnectivity. The absence of the glass transition at 280° C indicates that the lead-rich phase is totally crystallized. As PbSe and PbSe₂ crystallize from the Pb-rich, minor phase, the average composition of the uncrystallized part of the material is depleted in PbSe, thus increasing the volume fraction of the Pb-poor, major phase via the lever rule. This also decreases the Se

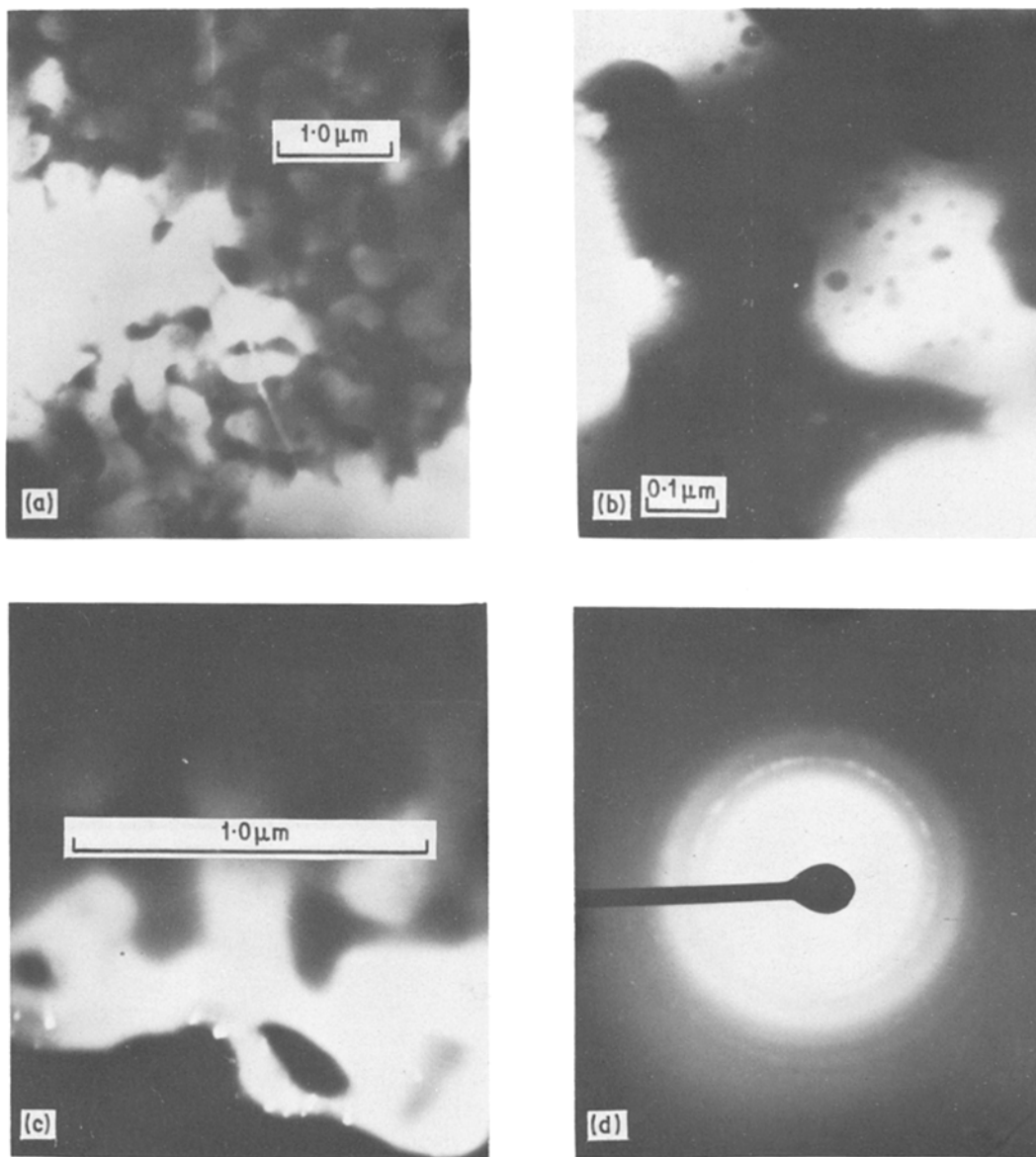


Figure 2 Transmission electron micrographs of 0.3 PbSe-0.7Ge_{1.5}As_{0.5}Se₃ glass, heat-treated at 350° C for 3h, quenched in air, and ion thinned. (a), (b) Direct transmission. (c) Dark field microscopy. (d) Electron diffraction.

content of the uncrystallized, major phase, which results in a shift of its T_g from $\sim 325^\circ\text{C}$ (Fig. 1) to $\sim 340^\circ\text{C}$ (Fig. 3).

Heat-treatments anywhere between about 335 and 400° C could produce the same microstructure and amount of crystallization, the required heat-treatment time decreasing with increasing temperature. Alternatively, an initial heat-treatment between about 335 and 350° C followed by crystal growth at $\sim 400^\circ\text{C}$ produced the same microstructure as a single heat-treatment in a

reasonably short time. Fig. 4 shows a typical two stage heat-treatment schedule with typical microstructure that is produced at different stages of crystallization. The micrograph for the crystallization cycle (Fig. 4) exhibits an almost completely crystallized ceramic microstructure with $\sim 0.7\ \mu\text{m}$ particle size.

3.1.1. Calculation of percentage crystallization from heat capacity data

The increases in heat capacity shown in Fig. 1,

DSC Trace of $0.3\text{PbSe} - 0.7\text{Ge}_{1.5}\text{As}_{0.5}\text{Se}_3$
Glass Heat-Treated at 350°C for 65 hours

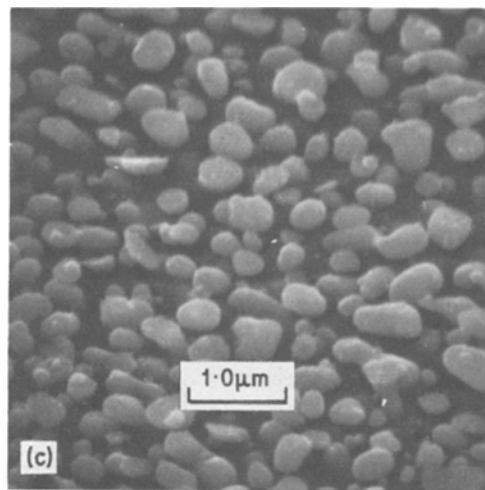
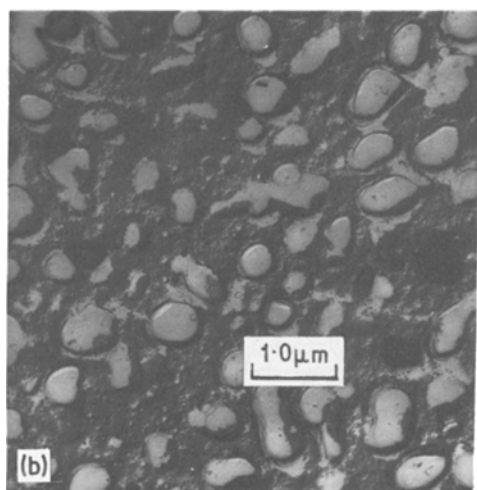
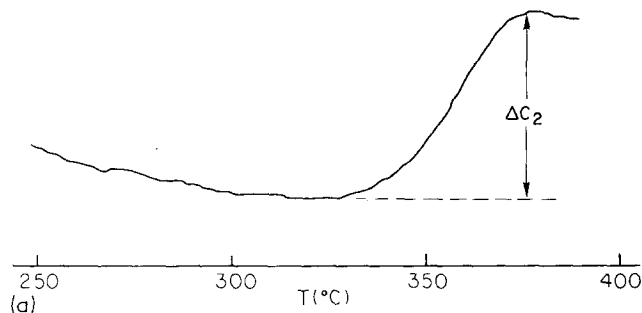


Figure 3 DSC trace and micrographs of $0.3\text{PbSe} - 0.7\text{Ge}_{1.5}\text{As}_{0.5}\text{Se}_3$ glass heat-treated at 350°C (a) for 65 h; (b) for 65 h, two stage replication; (c) for 95 h, SEM.

ΔC_1 and ΔC_2 , as measured by DSC, are due to the glass transitions of the respective phases 1 and 2. Crystals do not exhibit such transitions, which are due to the “unfreezing” of the liquid-like degrees of freedom of the glass. Consequently, if a phase undergoes crystallization, the magnitude of the heat capacity rise at its glass transition will decrease by an amount roughly proportional to the fraction crystallized.

In Fig. 5 the relative changes in the heat capacity breaks, $\Delta C_1/C_g$, $\Delta C_2/C_g$, and $(\Delta C_1 + \Delta C_2)/C_g$, are plotted as a function of heat-treatment time at 350°C , where C_g is the heat capacity measured below the lowest glass transition temperature (cf. Fig. 1). The fact that $\Delta C_1/C_g$ vanishes after 20 h heat-treatment indicates that the lower T_g (Pb-rich) phase is completely crystallized at times greater than 20 h. From the data of Fig. 5 one may make a rough

estimate of the percentage of the glass crystallized using the following equation:

$$\% \text{ crystallization} = 100 \left[1 - \frac{[(\Delta C_1 + \Delta C_2)/C_g]}{[(\Delta C_1 + \Delta C_2)/C_g]_0} \right]$$

where $[(\Delta C_1 + \Delta C_2)/C_g]_0$ is the value of this quantity for zero heat-treatment time, i.e. for the uncrystallized glass as quenched from the melt. Percentage crystallization calculated from this equation is plotted versus heat-treatment time in Fig. 6. Fig. 6 indicates that the product obtained after long heat-treatment times is about 50% crystallized, in reasonable agreement with volume fraction measurements from electron micrographs (cf. Fig. 4).

3.2. Effect of crystallization on infra-red transmission

Fig. 7 shows the infra-red spectra for the glass and

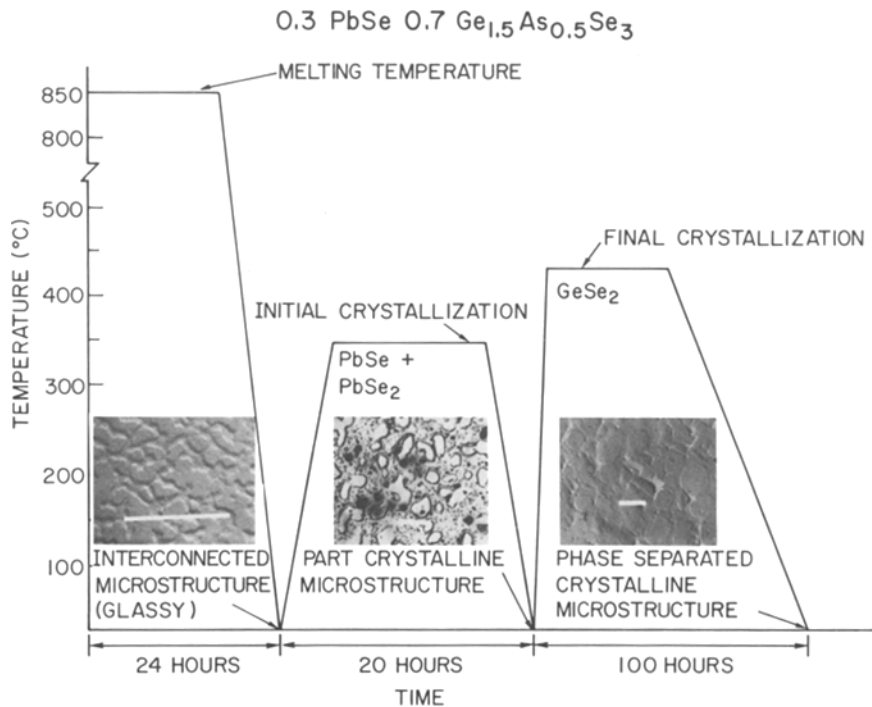


Figure 4 Typical heat-treatment schedules of 0.3 PbSe-0.7Ge_{1.5}As_{0.5}Se₃ glass with the resulting microstructure (two stage replicas) shown at each stage. Some glasses were heat-treated in one stage at the lower temperature for long times.

glass-ceramics as a function of heat-treatment. The low wavelength cut-off moves to longer wavelengths with crystallization due to the enhancement of absorption, because the crystallized phase has a lower band gap than the original phases. The change in slope that can be observed in the regions between the low wavelength cut-off and the relatively flat portion of each spectrum, respectively, is due to scattering by the crystalline particles.* Thus, the transmission at a given wavelength

decreases with increased crystallinity and increased particle size. The transmission in this region can be predicted by the Rayleigh scattering law, i.e. the transmission is proportional to λ^{-4} , where λ is the wavelength of the infra-red beam. Transmission losses in the flat region observed on the quenched melt spectrum (6 to 11 μ m) are mainly due to reflection. The extent of this region decreases markedly with heat-treatment due to crystallization and the growth in the isolated crystalline

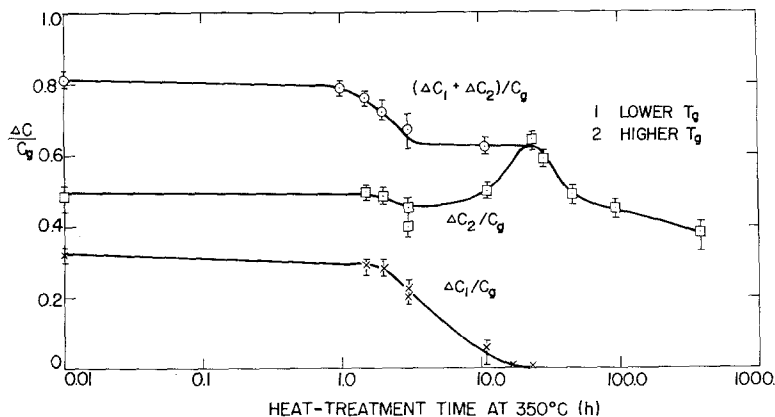


Figure 5 Relative change in heat capacity increase as a function of heat-treatment time at 350°C for 0.3 PbSe-0.7Ge_{1.5}As_{0.5}Se₃ phase-separated glass. The top line corresponds to the total amount of glass in the lead selenide-rich phase.

*For example, the interconnected particles of ~ 0.3 μ m for the parent glass grow to about 0.6 μ m isolated particles for a 24 h treatment at 400°C (~ 50% crystallization).

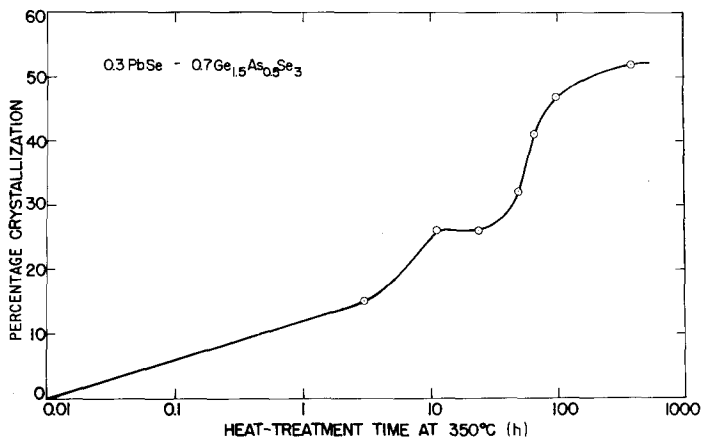


Figure 6 Percentage crystallization as a function of heat-treatment time at 350° C. The percentage was calculated from the data obtained in Fig. 5.

particles. The large absorption band at higher wavelengths ($\sim 12.8 \mu\text{m}$) is mainly due to the presence of oxide impurities and can be reduced by purification [17]. The absorption at the longest wavelengths ($> 15 \mu\text{m}$) is due to intrinsic 2-phonon absorption [5]. The absorption coefficient, α , at $10.6 \mu\text{m}$ (CO_2 laser wavelength) increases from 0.02 cm^{-1} for the quenched melt (determined by laser calorimetry [5]) to about 1 cm^{-1} for the glass-ceramic heat-treated at 400°C for 65 h.

3.3. Effect of crystallization on microhardness

The data (Table I) in this study generally indicates monotonically increasing microhardness with increasing crystallization. The microhardness increases until $\sim 26\%$ of the sample is crystallized, corresponding to ~ 28 volume fraction of the lead-rich phase and levels off until about 47% of the

entire sample is crystallized. This seems to suggest that only the fully crystallized phase of lead selenide crystals (smaller volume fraction) contributes to the microhardness until a significant amount of the major phase containing lead selenide and germanium selenide is crystallized.

3.4. Effect of crystallization on the fracture strength

The results of the modulus of rupture (MOR) tests conducted on the initial glass and four heat-treated samples are presented in Table I. A statistical analysis† demonstrated with over a 99% confidence level that the MOR of the $\sim 45\%$ and 60% crystallized glass-ceramics were ~ 60 and $\sim 100\%$ larger, respectively, than that of the uncrystallized glass.

Fracture surface analysis showed the expected increased roughness with increased crystallinity,

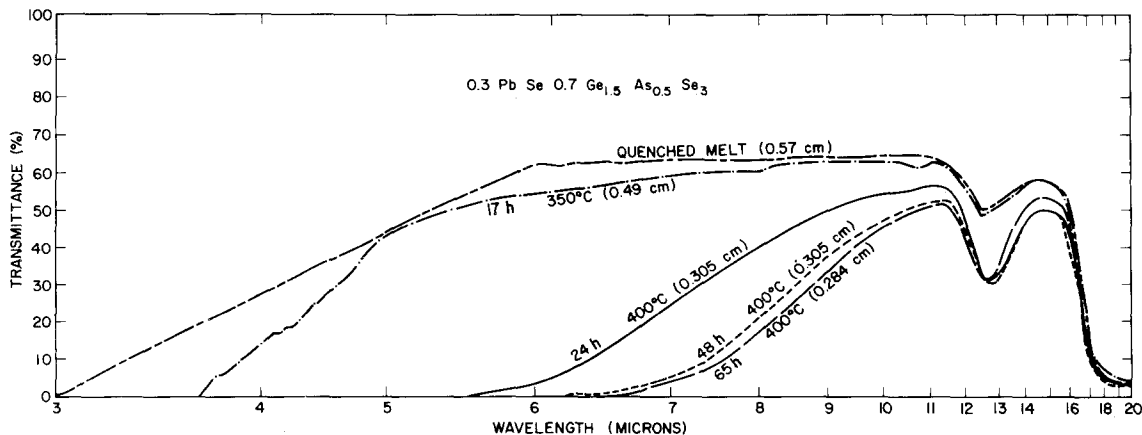


Figure 7 Infra-red transmission as a function of wavelength for various heat-treatments. Percentage crystallinity of samples: 17 h, 350° C - 26%; 24 h, 400° C - 46%; 48 h, 400° C - 50%; 65 h, 400° C - 55%. Numbers in parentheses in figure are sample thicknesses.

† Student's "t" comparison.

‡ The 43, 46 and 47% glass-ceramics taken as a group.

TABLE I Properties of 0.3PbSe–0.7 Ge_{1.5}As_{0.5}Se₃ glasses and glass-ceramics

Heat-treatment (°C, h)	% Crystallization	T_{g_1} (°C)	T_{g_2} (°C)	Vickers microhardness (100 g load) (kg mm ⁻²)	Failure stress* (MN m ⁻²) [psi × 10 ²]	Mirror constants† (MN m ^{-3/2})	
						A_i	A_o
Uncrystallized glass	0	280	325	216 ± 16	19 ± 5 (5) [28 ± 7]	0.31	0.39
350 – 3	16	280	325	244 ± 4			
350 – 24	26		340	250 ± 8			
350 – 48	32		347	234 ± 3			
350 – 65	43		337	250 ± 4	32 (1) [46]	0.50	0.60
400 – 17	46		332		31 ± 3 (6) [45 ± 5]	0.51	0.62
350 – 96	47		350	279 ± 13	31 ± 6 (4) [45 ± 8]	0.7	0.85
430 – 65	60		340	276 ± 7	38 ± 2 (2) [55 ± 2]	0.53	0.70

*No. of samples in parentheses, ± indicates 95% confidence limits.

† $A_i = \sigma r_i^{1/2}$ where r_i = inner mirror radius [14].

$A_o = \sigma r_o^{1/2}$ where r_o = outer mirror radius [14].

reflecting the increases in the number of paths available for the propagating crack (Fig. 8). Since the mirror constant A_i , elastic modulus E , and flaw half-width¶ b , were measured for several of the samples, the critical fracture energy, γ_c , can be determined [14, 15]:

$$\gamma_c = (b/r) \left[\frac{A^2}{Y^2 E} \right] \quad (1)$$

where Y is a geometric constant [18], and b/r is the flaw (half width) to mirror size ratio ($b/r \sim$

0.09) [14]. The calculation of the fracture energy demonstrated the expected increase from 0.8 J m⁻² for the glass to 1.5 J m⁻² for the ~ 50% crystallized glass-ceramic.

4. Conclusion

A fine grained (< 1 μm) chalcogenide glass-ceramic of the composition 0.3 PbSe–0.7 Ge_{1.5}As_{0.5}Se₃ has been produced from a phase-separated parent glass. The glass transition temperature was increased from 280 to 340° C by crystallizing the

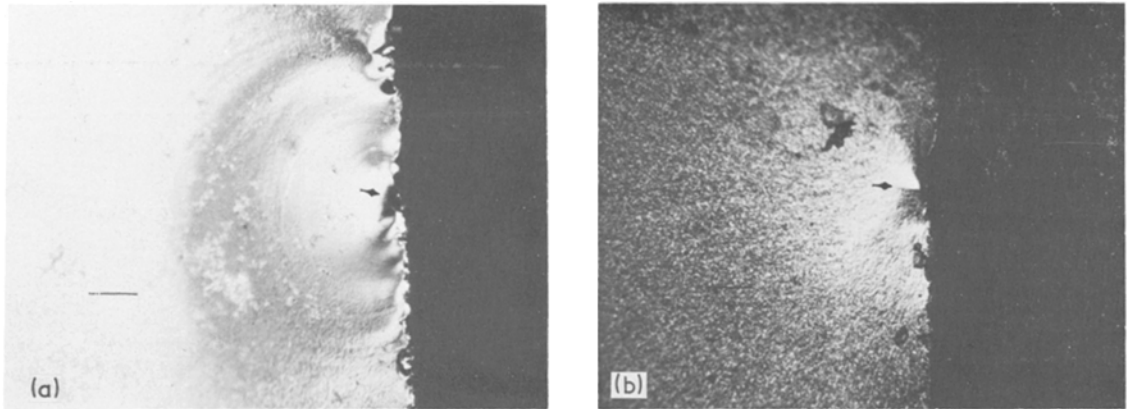


Figure 8 Optical photographs of the typical fracture surfaces of (a) glass and (b) glass-ceramic (17% crystalline) of 0.3 PbSe–0.7Ge_{1.5}As_{0.5}Se₃. Notice the approximately symmetrical, highly reflecting surface (inner fracture mirror) surrounding the fracture initiating flaw (arrow). Bar is 100 μm.

§ A is either the constant for the inner (i) or outer (o) mirror, cf. Table I.

¶These were approximately semi-circular flaws.

lower T_g phase of the glass. The infra-red transmission decreased with increased crystallization due to scattering and absorption by the crystalline particles.

The strength of the glass-ceramic increases with increased crystallization at least up to $\sim 60\%$ crystallinity, where the MOR was $\sim 100\%$ greater than the parent glass. The Vickers microhardness increases monotonically with increased crystallization within the interval measured.

Acknowledgements

The authors thank M. Samanta and A. Marshall for assistance in sample preparation. We also thank J. Wilder for DSC measurements and Dr M. Maklad for preparation and measurement of the infra-red transmitting discs. Special thanks are due Dr S.W. Freiman for many helpful discussions and review of the manuscript. The authors gratefully acknowledge the Office of Naval Research for sponsoring this research (Contract No. N00014-68-A-0506-002).

References

1. M. SPARKS, *J. Appl. Phys.* **42** (1971) 5029.
2. P. F. BECHER and R. W. RICE, Semi Annual Report No. 1, Naval Research Laboratory (ARPA Order No. 2031) (1972).
3. T. F. DEUTSCH, *J. Phys. Chem. Solids* **34** (1974) 2091.
4. L. L. BOYER, J. A. HARRINGTON, M. HASS and H. B. ROSENSTOCK, *Phys. Rev. B* **11** (1975) 1665.
5. C. T. MOYNIHAN, P. B. MACEDO, M. S. MAKLAD, R. K. MOHR and R. E. HOWARD, *J. Non-Crystalline Solids* **17** (1975) 369.
6. I. D. AGGARWAL, C. T. MOYNIHAN, P. B. MACEDO, J. J. MECHOLSKY and G. R. SRINIVASAN, *J. Amer. Ceram. Soc.* **55** (7) (1972) 366.
7. C. T. MOYNIHAN, P. B. MACEDO, I. D. AGGARWAL and U. E. SCHNAUS, *J. Non-Crystalline Solids* **6** (1971) 322.
8. G. H. BEALL, D. A. DUKE, *J. Mater. Sci.* **4** (1969) 34.
9. P. W. McMILLIAN, "Glass-Ceramics" (Academic Press, New York, 1964).
10. A. R. HILTON, *J. Non-Crystalline Solids* **2** (1970) 28.
11. U. E. SCHNAUS and C. T. MOYNIHAN, *Mater. Sci. Engr.* **7** (1971) 268.
12. J. J. MECHOLSKY, G. R. SRINIVASAN, C. T. MOYNIHAN and P. B. MACEDO, *J. Non-Crystalline Solids* **11** (1973) 331.
13. R. T. DeHOFF, in "Characterization of Ceramics" edited by L. L. HENCH and R. W. GOULD, (Dekker, New York, 1971) Ch. 18, p. 532.
14. J. J. MECHOLSKY, R. W. RICE and S. W. FREIMAN, *J. Amer. Ceram. Soc.* **57** (10) (1974) 453.
15. J. J. MECHOLSKY, S. W. FREIMAN and R. W. RICE, *J. Mater. Sci.* **11** (1976) 1310.
16. A. M. YEFIMOV and V. F. KOKORINA, *Sov. J. Opt. Tech.* **10** (Russ.) (1969) 43.
17. J. A. SAVAGE and S. NIELSON, *Infrared Physics* **5** (1965) 195.
18. G. R. IRWIN, *J. Appl. Mech.* **29** (*Trans. Amer. Soc. Mech. Engr.*) (December 1962) 651.

Received 10 November 1975 and accepted 24 February 1976.